Soft Matter

RSC Publishing

PAPER

View Article Online
View Journal | View Issue

Cite this: *Soft Matter*, 2013, **9**, 6091

Diffusivities, viscosities, and conductivities of solvent-free ionically grafted nanoparticles

Bingbing Hong and Athanassios Z. Panagiotopoulos*

Received 22nd March 2013
Accepted 17th May 2013

DOI: 10.1039/c3sm50832c

www.rsc.org/softmatter

A new class of conductive composite materials, solvent-free ionically grafted nanoparticles, were modeled by coarse-grained molecular dynamics methods. The grafted oligomeric counterions were observed to migrate between different cores, contributing to the unique properties of the materials. We investigated the dynamics by analyzing the dependence on temperature and structural parameters of the transport properties (self-diffusion coefficients, viscosities and conductivities) and counterion migration kinetics. Temperature dependence of all properties follows the Arrhenius equation, but chain length and grafting density have distinct effects on different properties. In particular, structural effects on the diffusion coefficients are described by the Rouse model and the theory of nanoparticles diffusing in polymer solutions, viscosities are strongly influenced by clustering of cores, and conductivities are dominated by the motions of oligomeric counterions. We analyzed the migration kinetics of oligomeric counterions in a manner analogous to unimer exchange between micellar aggregates. The counterion migrations follow the "double-core" mechanism and are kinetically controlled by neighboring-core collisions.

1 Introduction

Solvent-free liquids consisting of nanoparticles functionalized with oligomeric chains have attracted significant interest during the past decade.[1–4] Experiments and modeling suggest that their self-suspending, solvent-free character is a key determining factor for the structure and dynamics of these systems.[3,5–9] While progress has been made in theoretical understanding of the simpler versions of these systems, in which chains are covalently grafted on the particles giving rise to "Nanoscale Organic Hybrid Materials," there have been relatively few modeling attempts of their ionically grafted counterparts – often referred to as "Nanoparticle Ionic Materials" (NIMs). There are extensive experimental studies of NIMs with diverse core and counterion compositions.[10,11] The complex character of these materials results from their breakable ionic bonds, which render NIMs intermediate between covalently grafted and ungrafted polymer nanocomposite systems. Due to the strong electrostatic forces, ionically grafted nanoparticles are also expected to behave differently from neutral systems of grafted nanoparticles in free chains.[7,12,13] NIMs share features with charged colloids,[14] and have been characterized as ionic liquids with large, nanoscale ions,[15,16] or as nanoparticles covalently tethered to ionic liquids.[11,17–19] These analogies provide linkages of NIMs to more familiar systems, but each only captures one aspect of their character: either breakable grafting or charges. A simulation study is therefore necessary to clarify whether the actual behavior of ionically grafted nanoparticles is the result of a simple combination of these two factors, or determined by varying contributions of the underlying structural features, depending on the properties of interest.

Almost all experimental studies of ionically grafted nanoparticles have focused on rheological properties,[2,19–23] conductivities,[11,24] or a combination of the two.[1,17,18,25,26] Among these prior studies, ref. 10 and 27 are the most comprehensive, covering local to global dynamics of NIMs through analyses of dielectric spectroscopy, shear moduli, and viscosities. Diffusivities of NIMs have only been investigated in ref. 28. The effects of temperature on the dynamics have been thoroughly examined,[1,10,11,17–19,21–23,27] but only few experimental studies prepared a series of samples with modified oligomer lengths[25] or grafting densities.[2,27] The lack of systematic variation of parameters obscures underlying structure–property relations, while the absence of detailed data on all transport properties for a given system potentially masks their interdependence. In this simulation work, we attempt to address these two issues by (a) calculating all transport properties and analyzing counterion migration kinetics, which cover dynamics at different scales, in the same system, and (b) systematically altering temperature, chain lengths and grafting densities of NIMs and observing the effects on the dynamics.

There have been few computational or theoretical studies of ionically grafted nanoparticles to date. The most studied structures that exhibit similar core–shell ionic encapsulation

Department of Chemical and Biological Engineering, Princeton University, Princeton, NJ 08544, USA. E-mail: azp@princeton.edu

are polyoxometalate anions coupled with small[29,30] or dendrimeric[31] cations in solution. Prior work has paid close attention to morphologies, ion distributions, and water-mediated interactions between polyoxometalate anions, but not to the dynamics. Initial simulations of solvent-free NIMs have observed the migration of oligomeric counterions from one core to another[32] and have confirmed directly the conclusions from the experiments of Jespersen *et al.* on NIMs diffusion.[28] The measured diffusivity of polymeric counterions is larger by almost one order of magnitude than the estimation under the assumption that the core and its surrounding chain counterions move together as a hard sphere, so chains readily detach from nanoparticles.[28] However, the detachment and migration mechanism of the counterions are not clear. Visualization of simulation results in ref. 32 showed counterions moving freely between the surface charge sites on the same core, but detaching from the core only when a nearby core came close by. Of course, visualization only provides anecdotal evidence, and the possibility that some counterions leave the old core and enter the polymer matrix without the help from the approaching neighbors cannot be excluded. This provides a motivation for the present study to perform a quantitative analysis of chain migration kinetics, by analogy to exchanges of unimers between micellar aggregates. Micellar aggregates exhibit multiple mechanisms, including micelle collision and single-chain migration, each of which has a fully developed kinetic theory.[33–35]

In this work, we investigate diffusivities, viscosities, conductivities, and chain migration kinetics of solvent-free NIMs, as well as their relationships to temperature and structural parameters, in the hope to answer the issues raised in the previous paragraphs. We use the coarse-grained model from ref. 32, except that the size of nanoparticle cores is reduced to allow the systems to reach diffusive (long-time) behavior. This makes systematic studies of slow global relaxation related to viscosity and conductivity feasible. Details of the model and simulation approach are given in Section 2. Section 3 presents the results and highlights connections and contrasts between different dynamical property changes and migration mechanisms. We draw conclusions and outline possible future work in Section 4.

2 Model and simulation details

Fig. 1 shows the topology of the systems of interest, representing ionically grafted nanoparticles. In this model, there are solid nanoparticle spherical cores of diameter Δ and chains of m beads of diameter σ. Each nanoparticle core has g negatively charged surface sites located $(\Delta + \sigma)/2$ away from the core center. A core and its surface charge sites are treated as a rigid body.

Beads (or monomers) of the g counterion chains are connected by harmonic bonds, $U_b(r) = 1000\varepsilon(r - \sigma)^2/\sigma^2$, with one end bead carrying a unit of positive charge. Pairwise interactions between different types of particles (core–core, core–bead, and bead–bead) are described by a generalized Lennard-Jones potential:

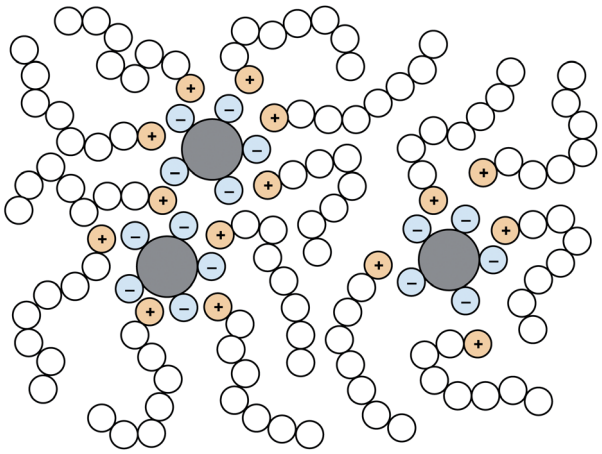

Fig. 1 Schematic of the systems of interest. The simulations are conducted in three-dimensional space, but a two-dimensional schematic is shown for clarity.

$$U_{\alpha\beta}(r) = 4\varepsilon\left[\left(\frac{\sigma}{r-\Delta_{\alpha\beta}}\right)^{12} - \left(\frac{\sigma}{r-\Delta_{\alpha\beta}}\right)^{6} + A_{\alpha\beta}\right] (r \le r_{\alpha\beta}) \quad (1)$$

For core–core and core–bead interactions, the potential is truncated at the minimum, $r_{\alpha\beta} = 2^{1/6}\sigma + \Delta_{\alpha\beta}$ and is purely repulsive, with constant $A_{\alpha\beta} = 1/4$. The shift distances ($\Delta_{\alpha\beta}$) are Δ and $\Delta/2$, respectively, for the core–core and core–bead interactions. No shift is used for the bead–bead interactions, $\Delta_{bb} = 0$; using $A_{bb} = (r_{bb}/\sigma)^{-6} - (r_{bb}/\sigma)^{-12}$, $r_{bb} = 2.5\sigma$, eqn (1) corresponds to a truncated and shifted Lennard-Jones potential. The same bead–bead potential also acts between charged surface and chain counterion sites. Note that we define core size in a different way from ref. 32. In ref. 32 nanoparticle diameter, d, equaled the distance at which core–core interaction disappears and consequently the distance between core and surface charges were $2^{1/6}\sigma$ larger; here we adopt instead $d = \Delta$ where the core–core potential goes to infinity, in order to match the location of the fist peaks in the core–core and core–bead radial distribution functions with the results obtained from atomistic simulations.[36]

To link the coarse-grained model to NIMs experiments where poly(oxyethylene) constitutes the majority of the organic phase, we mapped the critical parameters obtained in a Lennard-Jones fluid with interactions cut and shifted at 2.5σ (ref. 37) to the values for a virtual fluid of ethoxy units (CH_2OCH_2) estimated through the group contribution method of Constantinou and Gani.[38] This procedure gave $\sigma = 0.40$ nm, $\varepsilon/k_B = 377$ K, and the molar mass of beads was set to 44 g mol^{-1}. All data are converted to real units in the rest of the paper using these parameter values, to facilitate comparisons with experiments.

Surface and counterion beads have $-e$ and $+e$ charges, respectively, set by the fact that counterions commonly used in real NIMs systems are monovalent. In addition to the Lennard-Jones interaction described previously, charged beads also interact through Coulomb's law, $U_e(r) = q_i q_j/4\pi\varepsilon_0\kappa r$, where q denotes the charge, ε_0 is the dielectric permittivity of vacuum ($1/4\pi\varepsilon_0 = 8.988 \times 10^9$ N m^2 C^{-2}) and κ, the relative permittivity, is given the value of 4, appropriate for bulk silica.[39] Using a

relative permittivity corrects for the lack of polarizability of the nanoparticles and chains. Long-range electrostatic forces were calculated using the particle–particle–particle–mesh Ewald method with each charge extending 5 grid spacing and energy convergence tolerance of less than 10^{-4}.

The Large-scale Atomic/Molecular Massively Parallel Simulator (LAMMPS) package [40] was used to run simulations in cubic boxes with timestep $\Delta t = 6$ fs. Energy conservation within 0.05% was reported for model NIMs in *NVE* runs with $\Delta t = 12$ fs in ref. 32. We reduced the time step by half here to guarantee conservation over μs time scales. The core diameter was set to $\Delta = 0.902$ nm, similar to the size of polyoxometalate anions,[26] polyhedral oligomeric sisesquoxane (POSS) cage[41] and fullerenes,[23] which have been used in experiments as NIMs cores. The molar mass of the core particles was 505 g mol^{-1}, set in proportion to their volume ratio with respect to the chain beads. There were g = 4, 6, 8, 10, and 13 surface sites, and thus counterion chains, per core particle, corresponding to grafting densities from 1.6 to 5.1 nm^{-2}, within the range of grafting densities of the experimental systems. The "standard" system size investigated contained $N_C = 80$ core particles. Size effects were examined through simulations of systems of twice as many cores ($N_C = 160$) having the same core volume fractions. The larger systems have pressures, chain migration kinetics and conductivities identical within simulation uncertainties to those of the "standard" systems, but deviations of about 20% in the MSDs of the cores were observed.

To find a density (volume) corresponding to near-zero-pressure ($|P|$ < 45 bar at μs scale), we equilibrated systems at constant-volume conditions in different trial volumes for 12 ns, and measured the resulting pressure. It would have been simpler to perform constant-pressure simulations, but the version of LAMMPS we are using cannot handle rigid bodies when using barostats. After determining the system volume corresponding to zero pressure by interpolation of the initial runs, equilibration at that volume was performed for 30–60 ns, followed by a production period which lasted from 0.4 to 2.4 μs.

Table 1 lists the temperature T, chain length m, and number of surface beads per core, g, for each system simulated, as well as the resulting core volume fractions, $\phi = N_C V_C/V$, and reduced densities of polymer matrices, $\rho_m = \sigma^3(N_b + N_s)/(V - N_C V_C)$, after equilibration. Here, N_b, N_s, and N_C denote the total number of chain beads, surface charge beads and cores, respectively. V is the total volume of simulation box and V_C the volume of individual cores ($= 4\pi\Delta^3/24$, where $\Delta = 0.902$ nm). The conversion factor from ρ^* to real units is $\rho = 1.14 \times \rho^*$ [g cm^{-3}]; we provide ρ^* rather than ρ in this table to indicate the degree of packing of chain beads in the space between core particles in familiar Lennard-Jones units.

Mean square displacements (MSDs) of the cores and chains were monitored, and diffusivities were calculated as the slope of the MSDs in diffusive regimes,

$$D = \frac{1}{6}\lim_{t\to\infty}\frac{\mathrm{d}}{\mathrm{d}t}\left\langle[\mathbf{r}_i(t+t_0)-\mathbf{r}_i(t_0)]^2\right\rangle_{i,t_0} \quad (2)$$

here $\mathbf{r}_i(t)$ represents the position of center of a core particle, or center-of-mass of chain, i at time t. Both viscosities and conductivities reflect the relaxation of the entire melt. We applied the Green–Kubo relation for viscosity calculation (eqn (3)) in a volume V at temperature, T.

$$\eta = \frac{V}{k_B T}\int_0^\infty \left\langle P_{\alpha\beta}(t+t_0)P_{\alpha\beta}(t_0)\right\rangle_{t_0}\mathrm{d}t \quad (3)$$

$P_{\alpha\beta}$ is the off-diagonal element of the pressure tensor. Similar to the diffusivity, the conductivity was obtained as the derivative of the MSD of the collective translational dipole moment,[42,43] $\mathbf{M}(t)$.

$$\lambda = \frac{1}{6VTk_B}\lim_{t\to\infty}\frac{\mathrm{d}}{\mathrm{d}t}\left\langle[\mathbf{M}(t+t_0)-\mathbf{M}(t_0)]^2\right\rangle_{t_0} \quad (4)$$

where $\mathbf{M}(t) = \sum_{i=1}^{N_{ion}} q_i \mathbf{r}_i(t)$. Eqn (4) indicates either increasing the charges or enhancing the mobility of ions leads to a raised conductivity of the materials of interest.

The reasons we used the Einstein–Helfand formalism for diffusivity and conductivity, but the Green–Kubo formalism for the viscosity, are the large storage space requirements for the latter, and the fact that integration over recorded velocities for D or λ for the Green–Kubo relation is less accurate than directly using particle positions. For η, however, it is unclear how to remove the discontinuity in the Helfand moment caused by the electrostatic interaction changes when a particle jumps across the periodic boundaries;[44] the Green–Kubo method is boundary-condition-free and only requires inexpensive storage of pressure tensors.[45]

To quantify the counterion migration of NIMs, we first labelled half of the cores (denoted by C_m) in the melt and the chains that were originally attached to the marked cores. The number distribution of cores with n_l labeled chains, $Q(n_l, t)$, and the average number of labeled chains remaining on one marked core, $\langle n(t)\rangle$, were then recorded along the time. We compared the normalized decay of labeled chains per core,

$$x = \frac{\langle n(t+t_0)\rangle_{i_{C_m},t_0} - \langle n(\infty)\rangle_{i_{C_m},t_0}}{\langle n(t_0)\rangle_{i_{C_m},t_0} - \langle n(\infty)\rangle_{i_{C_m},t_0}} \quad (5)$$

Table 1 Parameters and equilibrium volumetric properties for the systems studied

T (K)	m	g	ϕ (%)	ρ^*_m
343	14	8	3.70	0.768
373	14	8	3.62	0.751
388	14	8	3.59	0.744
403	14	8	3.55	0.736
428	14	8	3.48	0.722
453	14	8	3.42	0.708
373	4	8	8.42	0.613
373	5	8	7.43	0.642
373	7	8	6.02	0.682
373	9	8	5.06	0.709
373	11	8	4.37	0.730
373	19	8	2.83	0.776
373	29	8	1.96	0.800
373	14	4	5.95	0.636
373	14	6	4.54	0.713
373	14	10	3.02	0.778
373	14	13	2.41	0.801

among different conditions. In Section 3 it is shown that few free (detached) counterions are observed in the melt, so $\langle n(t_0)\rangle_{i_{Cm},t_0} \approx g$, $\langle n(\infty)\rangle_{i_{Cm},t_0} \approx g/2$ and eqn (5) can be approximated by,

$$x \approx \frac{2}{g}\langle n(t+t_0)\rangle_{i_{Cm},t_0} - 1 \quad (6)$$

This virtual time-dependent process bears great similarity with many experiments[35,46] and theories[33,34] of unimer exchanges between micelles, which mix equal volumes of micelles formed by regular and probe molecules, respectively.

3 Results and discussion

3.1 Diffusivities

Even though the Coulombic potential between a charged surface site and a counterion bead at contact is up to $31k_BT$ in the temperature range of interest, the ionic bonds are breakable. Counterions and their attached chains can leave the cores with which they are initially associated, as seen previously.[32] The presence of electrostatic interactions slows down the diffusion of counterion beads – while in polymer melts the end monomers diffuse faster than the centers-of-mass of the chains at short times,[47] the opposite is the case for the MSDs of the charged end beads (dashed lines) relative to the chains (thin solid lines) in Fig. 2. In the diffusive regimes of the MSD curves in Fig. 2, the difference between the average displacements of chains and cores is >3 nm, larger than the core size, indicating the oligomeric counterions do not only move between anions on the same core, but jump to other cores, making the NIMs melts conductive.

Fig. 2 also shows that the effect of chain length on the short- and long-time diffusion behavior is somewhat counterintuitive. One generally expects that longer chains diffuse slower than short ones at both short and long times. Instead, it was observed that elongating NIMs oligomers from $m = 4$ to $m = 14$ reduces the core volume fractions from 8.4 to 3.6% and increases the density of oligomer matrix from 0.70 to 0.86 g cm^{-3}. Our previous simulations comparing the motions of covalently and ionically grafted nanoparticles at the same temperature and core volume fraction[32] also showed that the presence of charges significantly slows down the core motions. Thus, longer chains screen the strong core–core and core–counterion electrostatic interactions more effectively, making initial motions of cores and counterions faster. The long-time diffusion behavior is determined by relaxation of the polymer matrix, so that NIMs grafted with longer chains eventually become slower than those with short chains. Higher grafting densities result in slower long-time chain diffusion, due to the increased density of the chain matrix with ρ_m reaching 0.91 g cm^{-2} for $g = 13$, the highest grafting density studied.

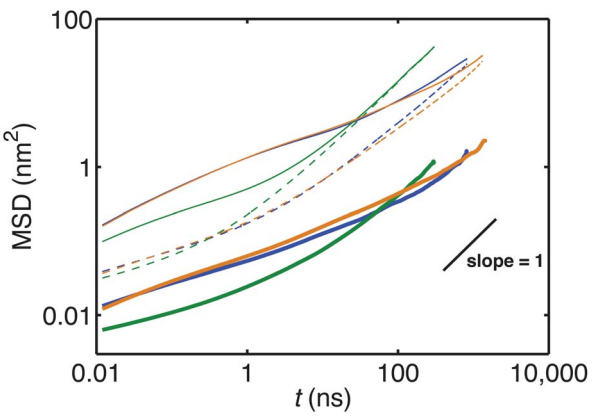

Fig. 2 MSDs of the cores (thick solid lines), centers-of-mass of chains (thin solid lines) and counterion beads (dashed lines) at $T = 373$ K. Blue: $m = 14$, $g = 8$; green: $m = 4$, $g = 8$; orange: $m = 14$, $g = 13$. The short black line of unit slope is shown for reference.

The effects of temperature and structural parameters on the long-time (diffusive) behavior are quantified in Fig. 3. The top panel shows a linear dependence of the logarithm of the self-diffusion coefficients of the cores and chains on $1/T$, which can be described by the empirical Arrhenius equation, $D = D_0\exp(E_d/k_BT)$. The good linearity observed suggests the simulated NIMs are far away from their glass transition temperature, T_g. Experimentally, pure poly(ethylene oxide) has a $T_g \approx -67$ °C.[49] NIMs systems have measured T_g's for SiO_2 cores with tertiary amines of −66 °C[27] and for ZrO_2 cores with linear $-(CH_2)_n-$ (ionic liquid) of −50 °C.[18] Exponential dependences of diffusivities for both anions and cations on $1/T$ were also obtained in previous MD simulations of ionic liquids in the range T = 300–400 K.[50,51] Ref. 50 estimated the activation energies for both ions of their ionic liquids and obtained E_d = 40–50 kJ mol^{-1}, on the same order of magnitude as the fitted activation energies of NIMs simulated in this paper, E_d = 53 kJ mol^{-1} for the cores and 37 kJ mol^{-1} for the chains. Jespersen *et al.*[28] measured the diffusivity of Jeffamine M-2070 ionically grafted to 18 nm nanoparticles through NMR relaxation. The measured value at 50 °C, (1.2–1.3) × 10^{-9} cm^2 s^{-1}, is of the same order of magnitude as the extrapolated D_m from simulations, 0.9 × 10^{-9} cm^2 s^{-1}. Jeffamine M-2070 is much longer than the simulated oligomers, thus expected to diffuse more slowly; but it has a lower charge density due to large core and chain sizes which works in the opposite direction.

In Fig. 3(b) the effects of chain length on the self-diffusion coefficients of the cores, D_C, and chains, D_m, are presented. The scaling factor of D_m with respect to m of around −1 suggests Rouse-like behavior[52] of the chains despite the confined geometry. We attribute this to the coarse-grained nature of NIMs model. Similar results have been observed in previous coarse-grained models of oligomer melts – softer potentials and longer bonds reduce the chain stiffness and shorten or even eliminate the "oligomeric" section before the Rouse regime.[9] The scaling theories for the unentangled polyelectrolytes in semidilute solutions predict the dynamics also follow the Rouse behaviors,[53] suggesting the presence of charges does not affect the chain dynamics under the simulated conditions. For the diffusion of cores, a nanoparticle smaller than the correlation length of the solvent, ξ, experiences the local "segmental viscosity", η_s, and diffuses independently of the chain length of the solvent.[54] For larger nanoparticles ($\Delta > \xi$) as in the simulations, the cores experience friction proportional to the number

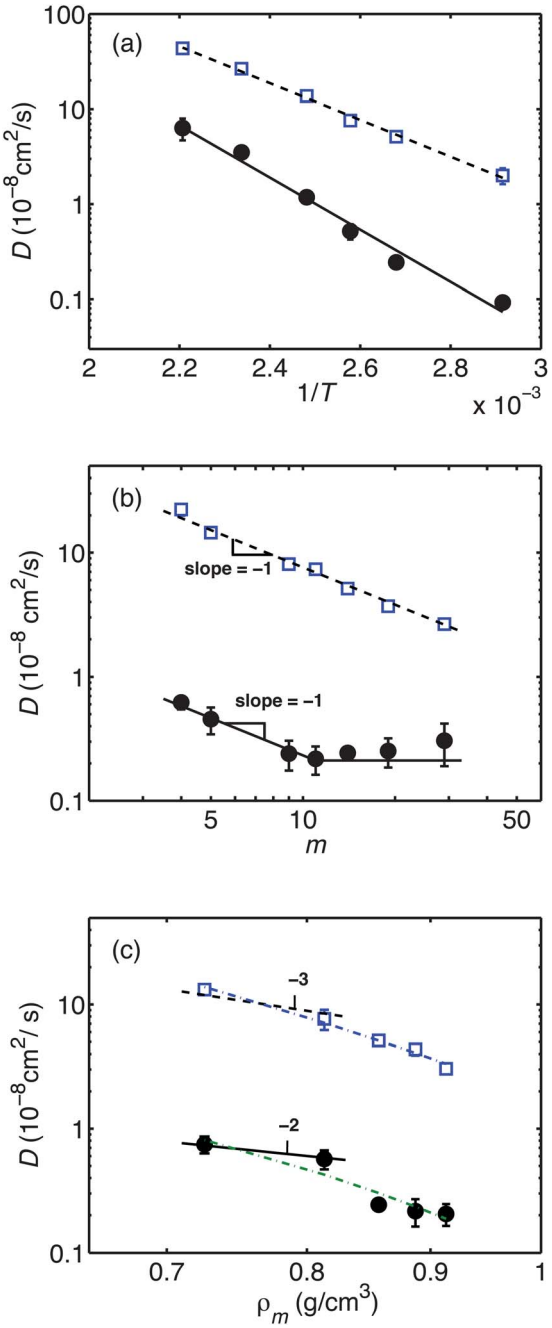

Fig. 3 Self-diffusion coefficients of the cores (solid circles), and chains (open squares) as functions of (a) inverse temperature for $m = 14$, $g = 8$, and (b) chain length m at $T = 373$ K, $g = 8$, and (c) number of surface charge sites g converted to matrix density ρ_m for $T = 373$ K, $m = 14$. Solid and dashed lines in (a) are Arrhenius expressions fitted to the cores and the chains, respectively. The dashed line in (b) is fitted to the Rouse model and the solid line to eqn (7) and the theory of ref. 48. In (c), the solid and dashed lines are based on the scaling theories of ref. 48 and the Rouse model, respectively; dash-dotted lines are fitted to $D = D_0\exp(-\alpha\rho_m)$.

of segments m/N_ξ, where N_ξ is the degree of polymerization corresponding to the correlation length.[48,54] So we have,

$$D_C \simeq \frac{k_B T}{\eta_s \Delta (m/N_\xi)} \sim m^{-1} \quad (7)$$

until the chain size becomes comparable to the size of nanoparticles at the degree of polymerization N_c. Further elongating the chains no longer changes the viscosity that the cores can "feel." Thus, the diffusivity of the cores remains almost constant when $m > N_c$.[48] In the simulation, D_C decreases as m increases and the dependence becomes weak above $m = 11$. The transition chain length is $N_c = 11$ and the transition size R_c of chains is then the hydrodynamic radius of the chain with $m = 11$. We estimate R_c through the polymer radius of gyration, $R_g = 0.536 \pm 0.003$ nm, and the empirical relation for linear flexible polymers,[55] $R_h \approx 0.75R_g$. The calculated transition size, $2R_c = 2R_h \approx 0.80$ nm, is very close to the core size. The same estimation for the chains with $m = 4$ leads to $2R_h = 0.44$ nm, roughly equal to the bead size σ. So the oligomers in the coarse-grained NIMs should have $\xi < \sigma$, or rather one bead is long enough to be an independent segment. This does not contradict the discussion above that the m dependence of chain diffusions follows the Rouse model. The fact that D–m relations in Fig. 3(b) can be well described with theories of polymer melts and nanoparticles in polymers confirms the conclusion drawn from the analysis of MSDs that ionic interactions only affect the short-time diffusion of cores and chains; at long times where the diffusion coefficients are calculated, motions are dominated by polymer relaxations.

By modifying the grafting density or the number of surface charges, g, we change the density in the oligomer matrix of NIMs, ρ_m. The dependence of the diffusion coefficients on ρ_m is given in Fig. 3(c). The matrix phase with varied density can be interpreted by analogy to polymer solutions, since ρ_m is proportional to the polymer concentration c. Scaling theories for polymer solutions give $D_m \sim \rho_m^{(\upsilon-2)/(3\upsilon-1)} \sim \rho_m^{-3}$,[52] and for nanoparticles in polymer solutions, $D_C \sim (1/\Delta^3)\rho_m^{-2\upsilon/(3\upsilon-1)} \sim \rho_m^{-2}$.[48] Both relations underestimate the observed dependences of diffusivities on the matrix density. We expect that the high concentration of the polymer matrix contributes to the steep D–ρ_m dependences, because in diffusion experiments of polystyrene solutions, slopes larger than $(2 - \upsilon)/(3\upsilon - 1)$ were observed if the concentration was further raised[56] after the semi-dilute regime. Exponential models have been tested to be a good describer of the D–ρ_m relation for chains[57] and nanoparticles[48,58] in solutions over wider concentration range. Adopting the expression $D \simeq D_0\exp[-\alpha\rho_m^{\upsilon/(3\upsilon-1)}] \sim \exp(-\alpha\rho_m)$ proposed in ref. 48, we generate good fits to both core and chain diffusions, obtaining $D_C = 0.23 \times 10^{-5}(\mathrm{cm^2\ s^{-1}})\exp(-7.75\rho_m)$ and $D_m = 3.39 \times 10^{-5}(\mathrm{cm^2\ s^{-1}})\exp(-7.58\rho_m)$.

3.2 Viscosities

Temperature effects on the viscosity of the model systems studied are plotted in Fig. 4(a). Arrhenius-type fitting, $\eta = \eta_0\exp(-E_\eta/k_BT)$, yields $E_\eta = 35$ kJ mol^{-1}, of the same order of magnitude as the calculated value (49–52 kJ mol^{-1}) for the ionic liquid 1-ethyl-3-methylimidazolium chloride in the temperature range 320–380 K in ref. 50. Experimental data for NIMs[22] composed of 5 nm TiO_2 nanoparticles and grafted by C_9H_{19}–C_6H_4–$(OCH_2CH_2)_{20}O(CH_2)_3SO_3^-$ are also plotted in

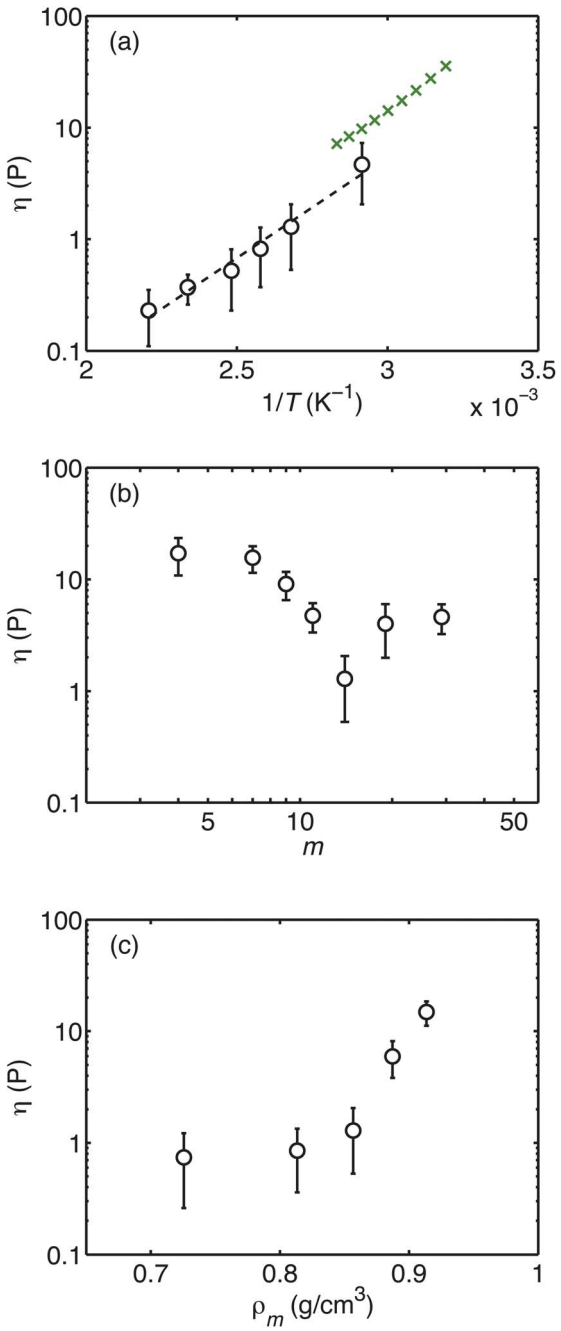

Fig. 4 (a) Temperature dependence of viscosities of simulated NIMs with $m = 14$, $g = 8$ (circles) and measured data for 5 nm TiO_2 grafted by C_9H_{19}–C_6H_4–$(OCH_2CH_2)_{20}O(CH_2)_3SO_3^-$ from ref. 22 (crosses). (b) Viscosities as a function of chain length for systems with $g = 8$ at $T = 373$ K. (c) Viscosity dependence on the matrix density (resulting from changes in g) for systems with $m = 14$ and $T = 373$ K.

Fig. 4(a) for comparison. Having larger core size and rigid benzene ring structures in the chains, this system has higher viscosities. The activation energy for the experimental systems is 37 kJ mol^{-1}, almost the same as the simulated NIMs. Comparing the model NIMs with their covalently grafted counterparts, POSS–$CH_2CH_2(OCH_2CH_2)_mOCH_3$,[8,41] the η–T activation energies for the latter with 10–30 w% cores are 30–40 kJ mol^{-1}, very near E_η of the model NIMs studied here. Thus, grafting with breakable ionic bonds or permanent, covalent ones, does not change the rate of viscosity rise with increasing temperature. Sticky Rouse models have been proposed, in which the zero-shear-rate viscosity is determined by the static modulus divided by the breakdown rate of linkages between sticky points.[59] The modulus is proportional to k_BT and the rate is $k_0 \exp(-W/k_BT)$, from which the viscosity is obtained to be essentially an exponential function of temperature. Because the experimental NIMs and the permanent grafted counterparts have similar activation energies, we conclude that stickiness in our model is related to penetration of chain coronas from neighboring cores, rather than the ionic bonds.

The effect of chain length on the viscosity of model NIMs is nonmonotonic as shown in Fig. 4(b). Two factors – core volume fraction and chain motions – compete in their effects on the system viscosity. For systems with shorter chains, there is a higher volume fraction of cores, as seen in Table 1, which in turn results in higher viscosity. Elongating the chains initially reduces the viscosity because it dilutes the cores. Over the range $m = 4$ to $m = 14$ viscosity changes by about one order of magnitude. Neither the conventional models for nanofluids in the form of $\eta/\eta_0 = 1 + 2.5\phi + f(\phi^2) + g(\phi^3)$ (η_0 is the base viscosity for the solvent),[60,61] nor the Krieger–Dougherty relation for charged colloids, $\eta/\eta_0 = (1 - \phi/\phi_m)^{-[\eta]\phi_m}$,[62] capture the large viscosity change seen in the simulations. The models generate only factors of 1.05–1.25 change in the ϕ range of interest (3–9%). As will be discussed in Section 3.4, many counterions are shared by neighbor cores, resulting in extended clusters. The highly viscous character of short-chain model NIMs likely results from the existence of the core clusters. If the chain becomes longer, core association is weakened, resulting in large viscosity reductions. The viscosity eventually increases again, due to the decreasing mobility of longer chains. Interestingly, the minimum in viscosity occurs at roughly the same chain length as the minimum in core diffusivity seen in Fig. 3(b). The same explanations can be applied for the drastic rise, by more than one order of magnitude, of viscosity when the number of grafted chains per core is increased, causing ϕ to vary from 2 to 6%, as displayed in Fig. 4(c). Increasing the number of surface charges enhances clustering of cores, resulting in larger viscosity rise than the models aforementioned predict. Although the coronas (or the matrix) is 26% denser, which is supposed to encapsulate cores from their neighbors better, the separation tend can not counterbalance the even stronger clustering effects.

3.3 Conductivities

We calculated the conductivities as the slope of the MSDs of collective translational dipole moments for all ions, $\mathbf{M}(t)$, in the diffusive regime (eqn (4)). Although related to the relaxation of the entire system, $\langle \Delta M^2(t) \rangle$ become diffusive (of unit slope) much earlier than the MSDs of individual cores. This can be easily explained if we expand eqn (4) into,

$$\lambda = \frac{1}{6Vk_BT}\frac{d}{dt}\lim_{t\to\infty}\sum_{i,j}^{N_{ion}} q_i q_j \langle \Delta\mathbf{r}_i \cdot \Delta\mathbf{r}_j \rangle$$
$$\sim \frac{1}{V}\left(N_{cat}{q_+}^2 D_{cat} + N_C{q_-}^2 D_C\right) \quad (8)$$
$$+\frac{d}{6Vdt}\lim_{t\to\infty}\sum_{i\neq j} q_i q_j \langle \Delta\mathbf{r}_i \cdot \Delta\mathbf{r}_j \rangle$$

where q_+ and q_- denote the charges carried by each cation and anion, respectively. At long enough times, $\Delta\mathbf{r}_i$ for different ions decorrelate, leading to $\langle \Delta\mathbf{r}_i \cdot \Delta\mathbf{r}_j \rangle = 0$. The diffusivity data in Fig. 3 show that counterions reach the diffusive regime within 10 ns for all systems studied, and that the diffusion coefficients for counterions, D_{cat}, are much larger than those of cores, D_C. Therefore, the conductivities or $\langle \Delta M^2(t) \rangle$'s are dominated by the diffusion term of cations,

$$\lambda \sim \frac{N_{cat}{q_+}^2}{V} D_{cat} \quad (9)$$

which reaches the diffusive regime around the same time as $\langle \Delta M^2(t) \rangle$ does. Eqn (9) will be further confirmed in subsequent discussion of λ.

As seen earlier for the self-diffusion coefficients and viscosities, the conductivities decrease exponentially as a function of $1/T$ over the temperature range simulated (Fig. 5(a)). Also included in Fig. 5(a) are experimentally measured conductivity data for polyoxometalates ionically grafted by tertially ammonium.[26] Having very close core size to the simulated nanoparticles (~1 nm), polyoxometalate-ammonium NIMs were measured to undergo a second-order transition around −35 °C. So the conductivities of the polyoxometalate liquid salts depend on temperature in the same Arrhenius manner as the simulated NIMs until the temperature drops down to out of the interested T range in simulations. The activation energies, E_σ, of the polyoxometalate salts and the simulated NIMs are both about 42–43 kJ mol^{-1}, almost the same as E_σ = 42–44 kJ mol^{-1} of the simulated and experimental ionic liquid, 1-ethyl-3-methylimidazolium chloride, in the range 325–489 K.[50,63] The comparison suggests that the slope of the log(conductivity) *versus* inverse temperature curves do not depend strongly on ion sizes. The absolute values of conductivities, however, are determined by the sizes of charge carriers, with ionic liquids of small ions being a thousand times more conductive than the simulated NIMs and polyoxometalate-ammonium salts.

To further analyze the ionic character of the simulated NIMs, we plot the molar conductivity (Λ) *vs.* the inverse viscosity, where $\Lambda = \lambda/c_+$ and c_+ is the mole concentration of positive charges, in comparison with the Walden's rule, $\Lambda\eta$ = constant, for strong electrolytes.[25,26,50,64] The Walden's rule can be obtained from the Einstein–Stokes equation, $D_i = k_BT/(6\pi\eta R_{h,i})$, and eqn (8) with no cross terms. The combination yields $\Lambda\eta = \sum C_i/R_{h,i}$ (C_i's are constants), free from temperature influences. The ideal Walden line is represented by dilute KCl aqueous solution (solid line in Fig. 5(b)) in which ions are fully dissociated and have equal mobilities.[64] Therefore $\log\Lambda$–$\log\eta^{-1}$ has a slope −1. Like other small salt solutions and ionic liquids,[50,64] the slope for the experimental polyoxometalate

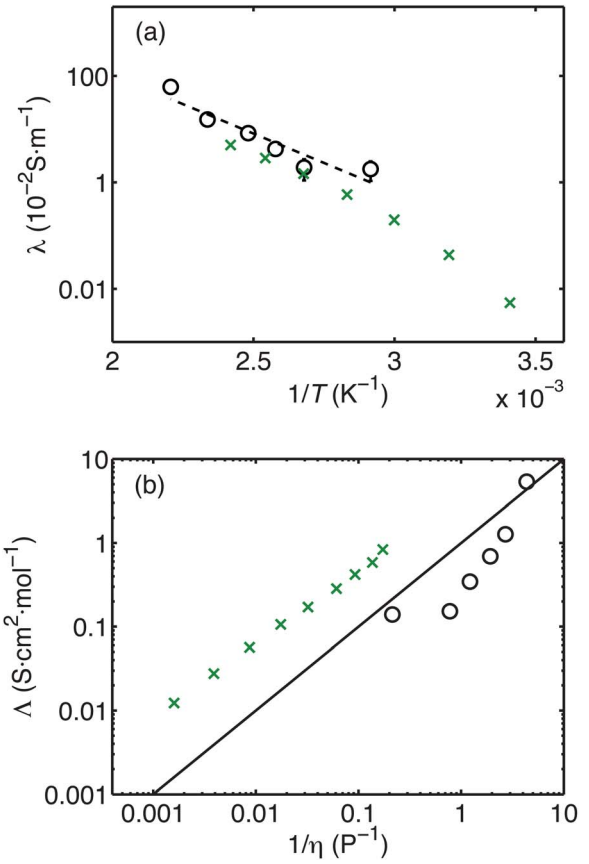

Fig. 5 (a) Temperature dependence of conductivity of simulated model NIMs with m = 14, g = 8 (circles) and polyoxometalates grafted by tertiary ammonium chains[26] (crosses); the dashed line is fitting to Arrhenius equation of the model NIMs data. (b) Walden plot of molar conductivity *versus* inverse viscosity for the simulated NIMs; the symbols are the same as in (a); the black line corresponds to dilute aqueous KCl solutions.

liquid salts is between 0 and 1.[26] In contrast, we observe >1 slopes in the model NIMs except for the point at the lowest temperature (or highest viscosity) which may be resulted from slow dynamics and poor statistics. Nugent *et al.*[25] reported similar >1 slopes for small electrolytes in covalently grafted nanoparticles, too. This trend is expected to rise from clustering between nanoparticles discussed in Section 3.2, which is also observed in covalently grafted nanoparticles.[5,8] As temperature drops, $\Lambda\eta$ is no longer constant due to the increasing hydrodynamic radius, $R_{h,i}$. Fig. 5(b) also illustrates the simulated NIMs are less ionic conductive than anticipated from their viscosities, compared with the superionic conductiveness (data points above the KCl line) of polyoxometalate salts and electrolytes/grafted nanoparticle mixtures in experiments. Better ionic conductance can be achieved by careful adjustment of the force fields for the NIMs model.

Fig. 6(a) illustrates that a power law is obeyed by conductivity as a function of chain length. The relation can be derived from eqn (9), which reflects the determining role of the chain motions with respect to the conductivities. Since each chain of length m carries a single charge, the charge density is proportional to m^{-1} at constant volume fraction of segments. However,

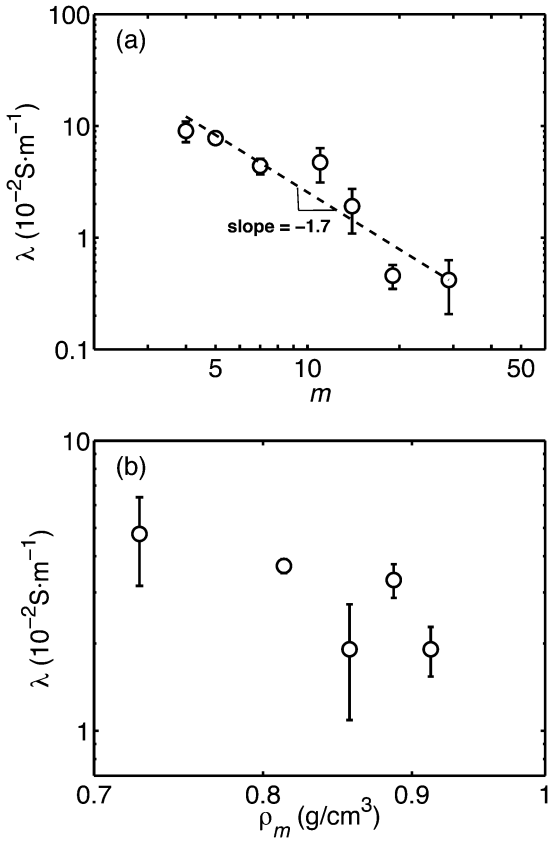

Fig. 6 Conductivities as a function of (a) chain length for $g = 8$ and $T = 373$ K and (b) number of grafting chains per core expressed through matrix density for $m = 14$ and $T = 373$ K. The dashed line in (a) has a slope of −1.7.

in our systems (simulated at constant pressure), the volume fraction of the matrix is not constant. Instead, data in Table 1 suggest an $m^{-0.7}$ dependence. The diffusion coefficients of cation end beads, equal to that of the chains, has been shown to be $\propto m^{-1}$ in Fig. 3(b). Substituting both into eqn (9), we derive the power for the conductivity dependence on chain length, $\lambda \propto m^{-1.7}$, seen in Fig. 6(a). Smaller changes in conductivity are brought by the modified grafting density in the simulated range, shown in Fig. 6(b). Despite large error bars, we can still observe the declining trend of conductivity with increasing number density of charge carriers in the system. As expressed in eqn (9), the conductivity is determined by two competing factors – charge mobilities and densities. Increasing charge density or proportionately ρ_m by 1.3 in the simulated range of g, the drop in diffusivity of chain ions (seen in Fig. 3(c)) is of a larger factor about 3. The combined effect is a decrease of conductivity by a factor 2.3, which is very close to the conductivity reduction in Fig. 6(b).

3.4 Counterion migration

There are two possible mechanisms for counterion migration, as discussed in the Introduction. The "single-core mechanism" assumes that counterion chains leave a core by internal interactions, *e.g.* steric repulsions or electrostatic interactions with its neighboring chains. The entry or exit rate of this mechanism is related to the concentrations of labeled chains attached to the old core and in the matrix. The "double-core mechanism" proposes that oligomeric counterions are transferred to neighboring cores only after two cores collide. The rate of migration to either of the two cores should incorporate the counterion concentrations on both cores.

We consider a counterion as being "bound" to a core particle when the distance between the counterion and any surface ion on the core is less than 0.65 nm. This is the distance corresponding to the first minimum in the radial distribution function for the ion pairs. Using this definition, we calculated the fractions of free chain cations and those shared by one or multiple nanoparticles. While the cations belonging to one and two cores vary between 40 and 60%, and cations shared by three cores take up about 10%, free chains are hardly found in the simulated systems. The absence of free chains strongly suggests that ionically grafted oligomers cannot leave one nanoparticle and enter the matrix on their own.

To obtain precise kinetic information, we conducted a virtual experiment by mixing equal numbers of "unlabeled" and "labeled" core particles, akin to experiments on micelle exchange experiments using time-dependent fluorescence[35] or SANS.[46] In the simulations, we know precisely the microscopic distribution of labeled molecules at any given time. We studied the time-dependent distribution of cores attached to n_l counterions, $Q(n_l, t)$. A shared counterion is judged to be attached to the core, any surface charge of which is closest to the counterion. Theoretically,[33,34] $Q(n_l, t)$ should approach the Poisson distribution (eqn (10)) as $t \to \infty$, irrespective of the initial distribution of labeled chains:

$$Q(n_l, \infty) = \frac{1}{n_l!} a^{n_l} \exp(-a) \tag{10}$$

The maximum of the distribution occurs at $n_l = a$. If the chains migrate between cores through diffusion in the matrix, $a = k_+[\text{chain}]/k_-$, where k_+ and k_- are the entry and exit rate constants for single chains and a is a function of temperatures and structural parameters. Consequently, we should observe changed locations and shapes of the equilibrium distributions of $Q(n_l, t)$ under different conditions. But Fig. 7 shows the calculated $Q(n_l, \infty)$ curves only depend on the grafting densities, which is in fact the characteristics of the "double-core" mechanism. The parameter a in eqn (10) is derived to be the average number of labeled chains each core has, or more exactly $a = g/2$ for the NIMs simulated, if the inter-core migrations of counterions only occur at the time when the cores contact each other. The separated peaks for NIMs having different g's in Fig. 7 are at the position predicted by the second mechanism. Moreover, the good overlap between $Q(n_l, \infty)$'s at different temperatures and chain lengths exclude the possibility that the "single core" mechanism contributes to the kinetics.

The evolution of $Q(n_l, t)$ are given in Fig. 8 together with the numerically integrated Q from Tachiya's two-core theory[34] starting from the simulated initial distributions. Due to the high percentage of chain ions shared by multiple cores, many cores are not in contact with the same number of counterions as

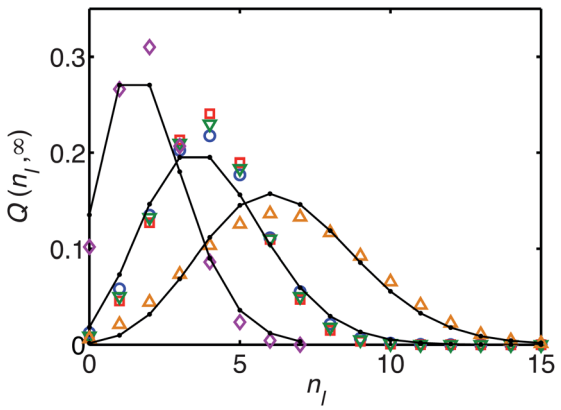

Fig. 7 Equilibrium distribution of cores having n_l labeled chains. Circles: $m = 14$, $g = 8$, $T = 373$ K; squares: $m = 14$, $g = 8$, $T = 453$ K; downward triangles: $m = 11$, $g = 8$, $T = 373$ K; diamonds: $m = 14$, $g = 4$, $T = 373$ K; upward triangles: $m = 14$, $g = 13$, $T = 373$ K. Lines are from eqn (10) with $a = 2$, 4, 6.5 from left to right.

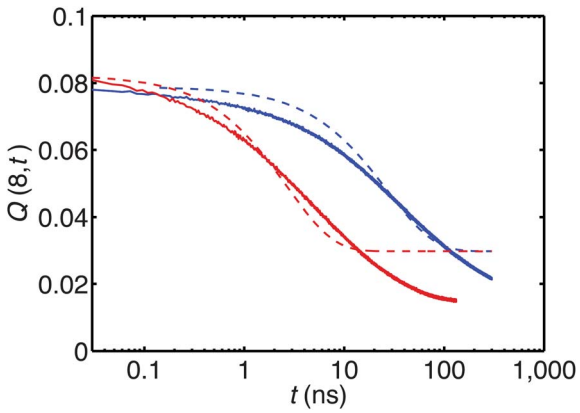

Fig. 8 Simulated (solid lines) and theoretical (dashed lines) evolution of the fractions of cores that have 8 labeled chains attached at 373 K (right curves) and 453 K (left curves). The theoretical curves are the numerical integrations of eqn (28) in ref. 34 with k set to be 2×10^{-4} at 373 K and 2×10^{-3} at 453 K.

the number of charge sites they carry. Thus, the initial fraction of cores attached by exactly g labeled chains is much less than 50%. For the theoretical curves, all the effects of temperature and other structural parameters are incorporated into the rate constant of hopping, k, for each chain. Modifications of k do not alter the shapes but shift the curves left- or right-wards. So the theory cannot capture complicated factors – for example, some chains take some time to move over the core surface to get to the contact point, from which they hop to the neighboring core. The time lags before hopping results in a distribution of the actual rate constant, which can bring changes to the slopes and improve the predictive ability of the theory, as discussed later in this section.

Instead of the whole spectrum of $Q(n_l, t)$, the normalized average number of labeled chains remaining on the marked cores, $x(t)$, defined by eqn (5), is used in the following discussion. The $x(t)$ relationship can be interpreted as a diffusive flow from high-concentration to low-concentration regions, which usually obeys first-order kinetics:

$$x(t) = \exp(-kt) \tag{11}$$

Since many factors contribute to the rate constant k, *e.g.*, chain relaxations at different length and time scales, core collisions, surface diffusion and waiting time before chain hopping, it is necessary to introduce a spectrum of relaxations into k that follows the Gaussian distribution, as done previously to describe polymer motions:[46,65]

$$x(t) = \int_{-\infty}^{\infty} p(\ln k)\exp(-kt)\mathrm{d}\ln k \tag{12}$$

$$p(\ln k) = \frac{1}{\sqrt{2\pi}\mu}\exp\left[-\frac{(\ln k - \langle \ln k\rangle)}{2\mu^2}\right] \tag{13}$$

Eqn (11)–(13) are suitable for fitting a wide range of decay curves, with the mean ($\langle \ln k\rangle$) controlling for location and the variance ($\mu_{\ln k}$) the slopes (see Fig. 9(a)). Their flexibility, however, may conceal the true kinetics, as the quality of fitting can be equally good in the assumption of second-order flow

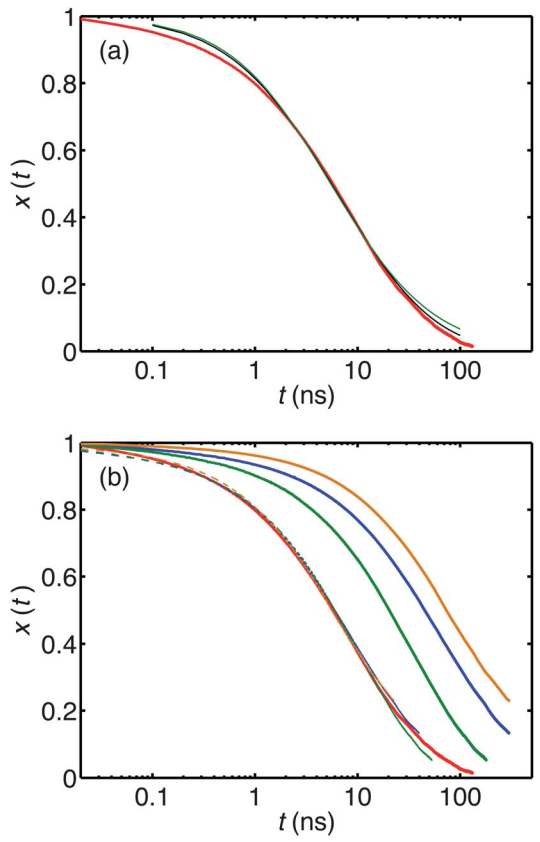

Fig. 9 Decay of the normalized number of labeled chains on each originally marked core. (a) Red: $m = 14$, $g = 8$, $T = 453$ K; black: fitting to 1st-order kinetics (eqn (11)–(13)) using $\langle \ln k\rangle = -2.2$ and $\mu = 1.4$; green: fitting to 2nd-order kinetics ($x(t) = 1/(kt + 1)$ and a spectrum of k expressed by eqn (13)) using $\langle \ln k\rangle = -1.7$ and $\mu = 0.8$; black and green lines almost overlap on the red line. (b) Blue solid: $m = 14$, $g = 8$, $T = 373$ K; red solid: $m = 14$, $g = 8$, $T = 453$ K; green solid: $m = 7$, $g = 8$, $T = 373$ K; orange solid: $m = 14$, $g = 13$, $T = 373$ K; dashed lines: shifted curves from those of the same color through dividing the time by a; dashed lines almost overlap the red solid line.

problem, $x(t) = 1/(kt + 1)$, combined with the Gaussian distribution of rate constant (eqn (13)). Fig. 9(b) displays an efficient way, which disregards the controversial kinetics involved, to obtain the relative relaxation times for migrations at all simulated conditions. Dividing the time in $x(t)$ by a factor a, we shift the decay curves leftwards by ln a to superpose a master curve. The factor a is proportional to the relaxation time or $1/k$.

The temperature-dependent shift factor a_T is presented in Fig. 10(a). Fitting Arrhenius equation to ln a_T and $1/T$ generates the activation energy $E_a = 34$ kJ mol^{-1}. The good linearity of the ln a_T–$1/T$ relation is consistent with the temperature dependence of the transport properties given in previous sections, but disagrees with the Rouse relaxation time $\sim m^2/(k_BT)$ adopted in Choi *et al.*'s experiments of micelle exchange.[46] Previous theoretical[66] and experimental works[65] that focused on the "single-core" mechanism of micelle systems have proposed and confirmed that the expulsion rate constant of polymers depends on the temperature in an Arrhenius manner. But for "double-core" mechanism, no previous efforts have been made to relate the rate constant to the temperature.

Fig. 10(b) displays the shift factor as a function of chain length together with the predictions from scaling theories. If a chain is expelled from a corona, leaving a core particle and entering the matrix by itself, the migration time should be proportional to the time it takes to diffuse through the corona, $\tau \sim L^3 f^{-1/2}(6\pi\eta_s)/(k_BT)$.[65,66] Here L is the thickness of the corona, and approximated by the height of a spherical brush, $L \sim d_g^{(1-\upsilon)/2} m^{\upsilon}$,[67] where d_g is the grafting density. The viscosity of solvents η_s can be independent on the chain length in the assumption that the cations just "feel" the friction of monomers, or $\eta_s \sim m$ if we continue to assume the Rouse dynamics for pure simulated chains. With υ set to 1/2, we obtain $a_m \sim m^{3/2}$ or $a_m \sim m^{1/2}$ for the two types of viscosities, respectively. Yet neither of the two scaling factors approximate the changing power of a_m–m well. In the "double-core" mechanism, the deterministic step for chain migration is that two neighbor cores diffuse through their corona layers until at least two charge sites from each core almost contact each other. Thus,

$$a_m \sim \tau \sim L^2/D_C \tag{14}$$

where we assume the distance between two neighbor cores is proportional to the height of spherical polymer brush. The diffusivities of cores follow $D_C \sim m^{-1}$ if $m < 11$, and is a constant for $m > 11$, as discussed in Section 3.1. Plugging D_C and L into eqn (14), we obtain,

$$a_m \sim \begin{cases} m^2 & (\text{small } m) \\ m & (\text{large } m) \end{cases} \tag{15}$$

Fig. 10(b) indicates eqn (15) gives a good prediction of the a_m–m scaling relation at the two extremes of short and long chains. As for the effect of grafting density shown in Fig. 10(c), we substitute the expression of spherical polymer brush and the exponential model for D_C from Section 3.1 into eqn (14), yielding $a_g = a_0[d_g(\rho_m)]^{1/2}\exp(7.75\rho_m)$. The good fits of this one-parameter expression and eqn (15) to the simulation data show in addition to the equilibrium distribution of labeled chains, the migration kinetics also follow the "double-core" mechanism.

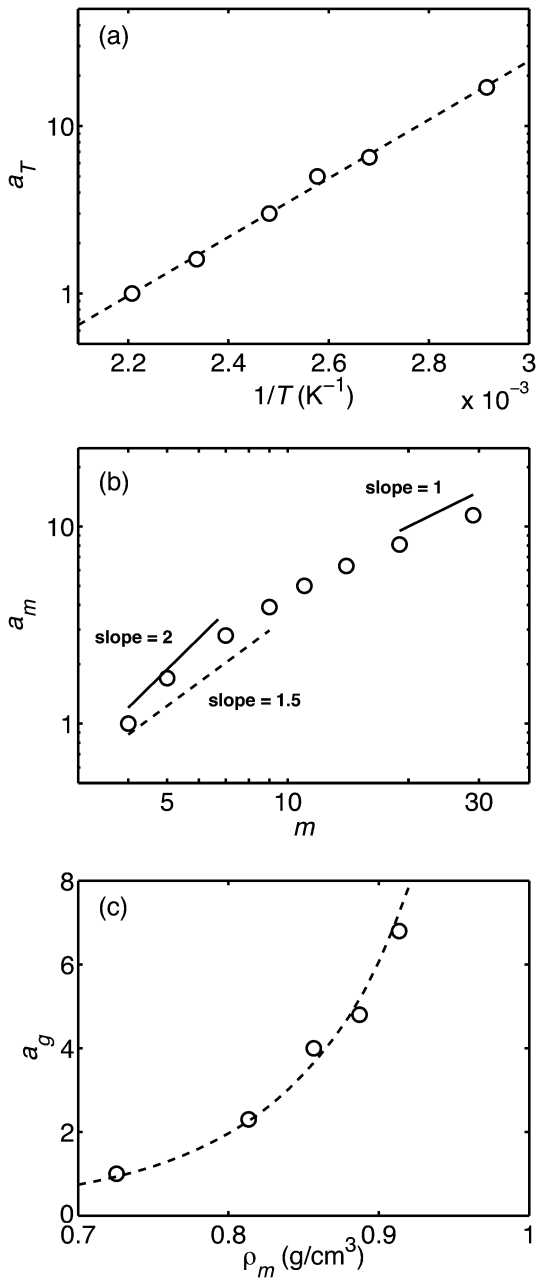

Fig. 10 The shift factors of the $x(t)$ decay curves as functions of temperature (a), and chain length (b), and matrix density modified through grafting density (c). (a) a_T is the shift factor for $m = 14$, $g = 8$ and varied T to the master curve $T = 453$ K; dashed curve is Arrhenius fitting. (b) a_m is the shift factor for $g = 8$, $T = 373$ K and varied m to the master curve $m = 4$. (c) a_g is the shift factor for $m = 14$, $T = 373$ K and varied g to the master curve $g = 4$; dashed curve is fitted to $a_g = a_0[d_g(\rho_m)]^{1/2}\exp(7.75\rho_m)$.

A remaining question is whether the "double-core" mechanism is still applicable if the strengths of electrostatic forces are varied. We have performed a calculation with permittivity $\kappa = 2$ and observed a slowdown of $X(t)$ by a factor of 4–5. This is expected, given that the breakdown of ionic bonds becomes slower and chain detachments occur less frequently. At the

other extreme, an increase in permittivity κ, or an increase of the effective size of the counterions, weaken electrostatic forces and may increase the possibility of "single-core" mechanism. This is an interesting topic for both experiments and simulations to explore whether the "single-core" mechanism can be observed in NIMs with weak electrostatic forces, *e.g.* conjugated oligomeric counterions which have large κ or dendritic-structured counterions that surround charges with thick layers of branched arms.

4 Conclusions

A coarse-grained molecular dynamics model for solvent-free ionically grafted nanoparticles has been developed. Detailed analyses of the dynamics of cores and chain ions, transport properties, and the migration kinetics of chains have been performed. Three key questions were addressed. The first one is whether melts of NIMs follow concepts valid for non-grafted particles in polymer melts (nanocomposites), covalently grafted nanoparticles, or ionic liquids. The diffusion data, especially the diffusivities of cores, display great similarity between the ionically grafted nanoparticles and polymer nanocomposites. Theories based on disconnections between cores and oligomers without taking the grafted structures or charges into account are sufficient to capture the diffusion dependence on chain length and temperature. With respect to viscosity, grafted structures and the presence of surface charges both exert effects through clustering effects. Conductivities of NIMs are dominated by oligomer diffusion, determined by the charges and the breakable ionic bonds. In the analysis of the migrations of chain counterions, we turn to the theories of micelles and polymer brushes, for which grafting and detachable structures become important. The second question relates to the connections between diffusivity, viscosity and conductivities in NIMs systems. A consistent dependence of the three transport properties, as well as the relaxation time of counterion migrations, is observed with respect to temperature. All properties follow Arrhenius-type relationships and show no indications of a glass transition. Changes in corona chain length and grafting density affect conductivities and migration relaxations in a manner that depends on the self-diffusion of either chains or cores. However, the dependences of viscosities on the structural parameters are unexpectedly strong. The last question is by what mechanism the oligomeric counterions migrate from one core to another. Data for the distributions of free ions and labeled chains, and the structural dependence of the relaxation times, all support the "double-core" mechanism. Counterions hop to neighbor cores through the contact point between the two cores and it is the time of diffusion of cores through the coronas that dominates the migration process.

The results of the present study were obtained under the assumption that the length scale of beads is that of ethoxy chemical units. With coarser mapping of model beads to longer segments, the simulated systems can also approximate NIMs comprised of larger nanoparticles and longer polymers. In an ongoing investigation, we are also studying model systems with larger core-to-bead diameter ratios. Because of slow dynamics, these systems require even more computational resources than the – already substantial – ones required for this work. Thus, the effect of core-to-bead size ratio will be investigated in a future publication. Besides the inter-core migration of chains discussed in this paper, the on-surface diffusion of counterions between the charge sites on the same core is also an interesting topic for future research. Suitable metrics need to be constructed to characterize the relative motions of ions and cores.

Acknowledgements

This publication is based on work supported by Award no. KUS-C1-018-02, made by King Abdullah University of Science and Technology (KAUST). Simulations were performed primarily on the Della cluster of the TIGRESS High Performance Computing Center at Princeton University. The authors would like to thank Profs. Emmanuel Giannelis, Lynden Archer, Donald Koch, Fernando Escobedo and Alissa Park for helpful discussions.

Notes and references

1 A. B. Bourlinos, R. Herrera, N. Chalkias, D. D. Jiang, Q. Zhang, L. A. Archer and E. P. Giannelis, *Adv. Mater.*, 2005, **17**, 234–237.
2 R. Rodriguez, R. Herrera, L. A. Archer and E. P. Giannelis, *Adv. Mater.*, 2008, **20**, 4353–4358.
3 P. Agarwal and L. A. Archer, *Phys. Rev. E: Stat., Nonlinear, Soft Matter Phys.*, 2011, **83**, 041402.
4 P. Agarwal, S. Srivastava and L. A. Archer, *Phys. Rev. Lett.*, 2011, **107**, 268302.
5 A. Chremos and A. Z. Panagiotopoulos, *Phys. Rev. Lett.*, 2011, **107**, 105503.
6 A. Chremos, A. Z. Panagiotopoulos, H.-Y. Yu and D. L. Koch, *J. Chem. Phys.*, 2011, **135**, 104901.
7 A. Chremos, A. Z. Panagiotopoulos and D. L. Koch, *J. Chem. Phys.*, 2012, **136**, 044902.
8 B. B. Hong and A. Z. Panagiotopoulos, *J. Phys. Chem. B*, 2012, **116**, 2385–2395.
9 B. B. Hong, A. Chremos and A. Z. Panagiotopoulos, *J. Chem. Phys.*, 2012, **136**, 204904.
10 A. B. Bourlinos, E. P. Giannelis, Q. Zhang, L. A. Archer, G. Flouda and G. Fytas, *Eur. Phys. J. E*, 2006, **20**, 109–117.
11 Y. Y. Lu, S. K. Das, S. S. Moganty and L. A. Archer, *Adv. Mater.*, 2012, **24**, 4430–4435.
12 S. Srivastava, P. Agarwal and L. A. Archer, *Langmuir*, 2012, **28**, 6276–6281.
13 J. L. Schaefer, S. S. Moganty, D. A. Yanga and L. A. Archer, *J. Mater. Chem.*, 2011, **21**, 10094–10101.
14 S. Bastea, *Soft Matter*, 2010, **6**, 4223–4228.
15 B. Smarsly and H. Kaper, *Angew. Chem., Int. Ed.*, 2005, **44**, 3809–3811.
16 B.-H. Han and M. A. Winnik, *Chem. Mater.*, 2005, **17**, 4001–4009.
17 Y. Y. Lu, S. S. Moganty, J. L. Schaefer and L. A. Archer, *J. Mater. Chem.*, 2012, **22**, 4066–4072.
18 S. S. Moganty, N. Jayaprakash, J. L. Nugent, J. Shen and L. A. Archer, *Angew. Chem., Int. Ed.*, 2010, **49**, 9158–9161.

19 S. S. Moganty, S. Srivastava, Y. Y. Lu, J. L. Schaefer, S. A. Rizvi and L. A. Archer, *Chem. Mater.*, 2012, **24**, 1386–1392.
20 D. Kim and L. A. Archer, *Langmuir*, 2011, **27**, 3083–3094.
21 P. Agarwal, H. B. Qi and L. A. Archer, *Nano Lett.*, 2010, **10**, 111–115.
22 A. B. Bourlinos, S. R. Chowdhury, R. Herrera, D. D. Jiang, Q. Zhang, L. A. Archer and E. P. Giannelis, *Adv. Funct. Mater.*, 2005, **15**, 1285–1290.
23 N. Fernandes, P. Dallas, R. Rodriguez, A. B. Bourlinos, V. Georgakilas and E. P. Gianellis, *Nanoscale*, 2010, **2**, 1653–1656.
24 X.-L. Hu, G.-M. Hou, M.-Q. Zhang, M.-Z. Rong, M.-Z. Rong, W.-H. Ruan and E. P. Giannelis, *J. Mater. Chem.*, 2012, **22**, 18961.
25 J. L. Nugent, S. S. Moganty and L. A. Archer, *Adv. Mater.*, 2010, **22**, 3677–3680.
26 A. B. Bourlinos, K. Raman, R. Herrera, Q. Zhang, L. A. Archer and E. P. Giannelis, *J. Am. Chem. Soc.*, 2004, **126**, 15358–15359.
27 R. Rodriguez, R. Herrera, A. B. Bourlinos, R. P. Li, A. Amassian, L. A. Archer and E. P. Giannelis, *Appl. Organomet. Chem.*, 2010, **24**, 581–589.
28 M. L. Jespersen, P. A. Mirau, E. von Meerwall, R. A. Vaia, R. Rodriquez and E. P. Giannelis, *ACS Nano*, 2010, **4**, 3735–3742.
29 A. Chaumont and G. Wipff, *J. Phys. Chem. C*, 2009, **113**, 18233–18243.
30 X. López, J. J. Carbó, C. Bo and J. M. Poblet, *Chem. Soc. Rev.*, 2012, **41**, 7537–7571.
31 R. Brodbeck, T. Tönsing, D. Andrae and D. Volkmer, *J. Phys. Chem. B*, 2008, **112**, 5153–5162.
32 B. B. Hong, A. Chremos and A. Z. Panagiotopoulos, *Faraday Discuss.*, 2012, **154**, 29–40.
33 M. Tachiya, *Chem. Phys. Lett.*, 1975, **33**, 289–292.
34 M. Tachiya and M. Almgren, *J. Chem. Phys.*, 1981, **75**, 865–870.
35 M. Hilczer, A. V. Barzykin and M. Tachiya, *Langmuir*, 2001, **17**, 4196–4201.
36 Before building the coarse-grained model, we tried atomistic NIMs consisting of POSS cores grafted by $-O^{-+}NH_4CH_2O(CH_2CH_2O)_nCH_3$. The same force fields as in ref. 8 were employed for POSS, $-O(CH_2CH_2O)_nCH_3$ and non-electrostatic interaction parameters for surface oxygen anions and α-CH_2's in the chains. The force parameters for ammonium groups and the partial charges assigned to α-C's were chosen from OPLS-AA (W. L. Jorgensen, *et al.*, *J. Phys. Chem.*, 1986, **90**, 2174–2182; W. L. Jorgensen, *et al.*, *J. Am. Chem. Soc.*, 1996, **118**, 11225–11236). Finally, the charges on the surface oxygen anions were set to meet the neutrality of the entire system.
37 B. Smit, *J. Chem. Phys.*, 1992, **96**, 8639–8640.
38 L. Constantinou and R. Gani, *AIChE J.*, 1994, **40**, 1697–1710.
39 P. R. Gray, P. J. Hurst, S. H. Lewis and R. G. Meyer, *Analysis and Design of Analog Integrated Circuits*, Wiley, New York, 5th edn, 2009, p. 40.
40 S. J. Plimpton, *J. Comput. Chem.*, 1995, **117**, 1–19.
41 K.-Y. A. Lin and A.-H. A. Park, *Environ. Sci. Technol.*, 2011, **45**, 6633–6639.
42 C. Schröder, C. Wakai, H. Weingärtner and O. Steinhauser, *J. Chem. Phys.*, 2007, **126**, 084511.
43 C. Schröder, M. Haberler and O. Steinhauser, *J. Chem. Phys.*, 2008, **128**, 134501.
44 S. Viscardy, J. Servantie and P. Gaspard, *J. Chem. Phys.*, 2007, **126**, 184512.
45 B. B. Hong, F. Escobedo and A. Z. Panagiotopoulos, *J. Chem. Eng. Data*, 2010, **55**, 4273–4280.
46 S.-H. Choi, T. P. Lodge and F. S. Bates, *Phys. Rev. Lett.*, 2010, **104**, 047802.
47 K. Kremer and G. S. Grest, *J. Chem. Phys.*, 1990, **92**, 5057–5086.
48 L.-H. Cai, S. Panyukov and M. Rubinstein, *Macromolecules*, 2011, **44**, 7853–7863.
49 S. Swier, R. Pieters and B. van Mele, *Polymer*, 2002, **24**, 3611–3620.
50 C. Rey-Castro and L. F. Vega, *J. Phys. Chem. B*, 2006, **110**, 14426–14435.
51 O. Borodin and G. D. Smith, *J. Phys. Chem. B*, 2006, **110**, 11481–11490.
52 M. Doi and S. F. Edwards, *The Theory of Polymer Dynamics*, Oxford University, New York, 1986, pp. 96 and 170.
53 A. V. Dobrynin, R. H. Colby and M. Rubinstein, *Macromolecules*, 1995, **28**, 1859–1871.
54 F. B. Wyart and P. G. de Gennes, *Eur. Phys. J. E: Soft Matter Biol. Phys.*, 2000, **1**, 93–97.
55 P. Somasundaran, *Encyclopedia of Surface and Colloid Science*, CRC Press, New York, 2nd edn, 2006, vol. 1, p. 4147.
56 T. Cherdhirankorn, A. Best, K. Koynov, K. Peneva, K. Muellen and G. Fytas, *J. Phys. Chem. B*, 2009, **113**, 3355–3359.
57 G. D. J. Phillies and D. Clomenil, *Macromolecules*, 1993, **26**, 167–170.
58 R. I. Cukier, *Macromolecules*, 1984, **17**, 252–255.
59 F. Tanaka and S. F. Edwards, *J. Non-Newtonian Fluid Mech.*, 1992, **43**, 247–271.
60 C. T. Nguyen, F. Desgranges, G. Roy, N. Galanis, T. Mare, S. Boucher and H. A. Mintsa, *Int. J. Heat Fluid Flow*, 2007, **28**, 1492–1506.
61 M. Hosseini and S. Ghader, *J. Mol. Liq.*, 2010, **153**, 139–145.
62 I. M. Krieger and T. J. Dougherty, *Trans. Soc. Rheol.*, 1959, **3**, 137–152.
63 A. A. Fannin, D. A. Floreani, L. A. King, J. S. Landers, B. J. Piersma, D. J. Stech, R. L. Vaughn, J. S. Wilkes and J. L. Williams, *J. Phys. Chem.*, 1984, **88**, 2614–2621.
64 W. Xu, E. I. Cooper and C. A. Angell, *J. Phys. Chem. B*, 2003, **107**, 6170–6178.
65 R. Lund, L. Willner, D. Richter and E. E. Dormidontova, *Macromolecules*, 2006, **39**, 4566–4575.
66 A. Halperin and S. Alexander, *Macromolecules*, 1989, **22**, 2403–2412.
67 K. Binder and A. Milchev, *J. Polym. Sci., Part B: Polym. Phys.*, 2012, **50**, 1515–1555.

